Temperature and load-ratio dependent fatigue-crack growth in the CrMnFeCoNi high-entropy alloy

Keli V. S. Thurston[a,b], Bernd Gludovatz[c], Qin Yu[a], Guillaume Laplanche[d], Easo P. George[e,f] and Robert O. Ritchie[a,b,*]

[a]Materials Sciences Division, Lawrence Berkeley National Laboratory, Berkeley, California 94720, USA
[b]Department of Materials Science & Engineering, University of California, Berkeley, California, 94720, USA
[c]School of Mechanical and Manufacturing Engineering, UNSW Sydney, NSW 2052, Australia
[d]Institut für Werkstoffe, Ruhr-Universität Bochum, D-44801, Bochum, Germany
[e]Materials Science and Technology Division, Oak Ridge National Laboratory, Oak Ridge, Tennessee 37831, USA
[f]Department of Materials Science and Engineering, University of Tennessee, Knoxville, Tennessee 37996, USA
*Corresponding author (roritchie@lbl.gov)

ABSTRACT

Multiple-principal element alloys known as high-entropy alloys have rapidly been gaining attention for the vast variety of compositions and potential combinations of properties that remain to be explored. Of these alloys, one of the earliest, the 'Cantor alloy' CrMnFeCoNi, displays excellent damage-tolerance with tensile strengths of ~1 GPa and fracture toughness values in excess of 200 MPa√m; moreover, these mechanical properties tend to further improve at cryogenic temperatures. However, few studies have explored its corresponding fatigue properties. Here we expand on our previous study to examine the mechanics and mechanisms of fatigue-crack propagation in the CrMnFeCoNi alloy (~7 μm grain size), with emphasis on long-life, near-threshold fatigue behavior, specifically as a function of load ratio at temperatures between ambient and liquid-nitrogen temperatures (293 K to 77 K). We find that ΔK_{th} fatigue thresholds are decreased with increasing positive load ratios, R between 0.1 and 0.7, but are increased at decreasing temperature. These effects can be attributed to the role of roughness-induced crack closure, which was estimated using compliance measurements. Evidence of deformation twinning at the crack tip during fatigue-crack advance was not apparent at ambient temperatures but seen at higher stress intensities (ΔK ~ 20 MPa√m) at 77 K by *post mortem* microstructural analysis for tests at R = 0.1 and particularly at 0.7. Overall, the fatigue behavior of this alloy was found to be superior, or at least comparable, to conventional cryogenic and TWIP steels such as 304L or 316L steels and Fe-Mn steels,; these results coupled with the remarkable strength and fracture toughness of the Cantor alloy at low temperatures indicate significant promise for the utility of this material for applications at cryogenic environments.

Keywords: High-entropy alloys; fatigue; crack propagation; temperature effects; load ratio; crack closure

1. Introduction

The notion of multiple-principal element alloys, specifically high-entropy alloys (HEAs), continues to captivate the structural materials community with the potential of innumerable new metallic alloys with a broad range of structural properties yet to be investigated [1-9]. In contrast to conventional alloy systems which invariably contain one, or two, principal elements, such as iron in steel or nickel in certain superalloys, HEAs were originally defined with a nominally equiatomic composition where the configuration entropy associated with at least five base elements was presumed to overwhelm the enthalpy of phase formation to create a (meta)stable solid solution [4,8,10]. Although more recent studies have since disputed this claim, the nomenclature has stayed and represents a highly active field of endeavor as new compositions are discovered [8,11-13].

A particularly notable HEA is the transition metal-based 'Cantor alloy' CrMnFeCoNi, a single-phase, face-centered cubic (*fcc*) solid-solution alloy which displays exceptional mechanical properties [2,11,14]. This alloy shows tensile strengths upwards of ~ 1 GPa, tensile ductilities of ~60 to 70%, and high fracture toughness values exceeding 200 MPa√m, which are further enhanced at cryogenic temperatures [14-17], properties that are comparable to, or exceed, those of cryogenic steels [15-18].

While the uniaxial tensile and toughness properties of CrMnFeCoNi and other high-entropy alloys are now well characterized [1-18], corresponding studies on the fatigue properties are sparse, despite the fact that potential applications of these alloys as future structural materials will invariably depend upon their fatigue resistance, which dictates component lifetimes. Prior work on the Cantor alloy has provided measurements of the high-cycle fatigue behavior of recrystallized CrMnFeCoNi at a single load ratio at 293 and 198 K [19] whereas other studies on cast Al-containing CrCoNi-based variants have focused on stress-life and crack propagation behavior [20,21]. These studies, while limited to ambient temperature testing conditions, have observed fatigue behavior comparable or superior to steels and other conventional alloys under both total-life and damage-tolerant fatigue testing, although this behavior may in part be attributed to their as-cast microstructures [20].

In the current work, we seek to extend our understanding of the fatigue behavior of these alloys and build upon our initial foundation [19] to further evaluate the near-threshold and fatigue-crack propagation behavior of polycrystalline CrMnFeCoNi under a broader range of conditions, specifically a range of load ratios with further cryogenic studies at 198 K and 77 K.

2. Experimental procedures

2.1. Mechanical testing

High-purity elemental constituents in near-equiatomic proportions were vacuum induction melted and cast to form a 40 mm diameter cylindrical ingot of CrMnFeCoNi. Once cast, the ingot was sealed in a silica casing and thermally homogenized at 1473 K for 48 hr. The ingot was then rotary swaged at room temperature to a final diameter of ~16.5 mm and recrystallized at 1073 K for 1 hr, yielding a final grain size of 7 ± 3 μm with a random orientation distribution [21]. The bulk material was then cut into disc-shaped compact tension (DC(T)) samples in accordance with ASTM Standard E1820 through electric discharge machining (EDM). Twenty-two samples were machined with the following dimensions: width W = 12.4 mm, thickness B = 6 mm, and initial notch length a_o = 3.6 mm with approximate notch root radii of ~100 μm, thus corresponding to an initial a_o/W ratio of ~0.28.

Once cut, the samples were manually polished using metallographic silicon carbide paper to a 1-μm mirror finish to allow for optical crack-length measurement. For continual monitoring of the crack-growth rate during testing, a linear patterned strain gauge (Vishay Precision Group, Raleigh, NC, USA) was used on the back-face of each specimen; model EA-06-031DE-350 gauges were used for tests at 293 K or 198 K and model WK-13-031DE-350 gauges at 77 K; the latter to permit accurate readings in the deep-cryogen environment. Crack lengths were calculated from the strain gauge readings of the elastic unloading portion of each cycle using the compliance expression for the DC(T) sample with back-face strain, as described by Ritchie *et al*. [23]:

$$a/W = 0.796239 + 5.40205u - 103.821u^2 + 714.676u^3 - 2603.44u^4 + 4829.01u^5 - 3578.51u^6 \quad , \qquad (1)$$

$$\text{where} \qquad u = \frac{1}{\sqrt{-EBCW}+1} \quad . \qquad (2)$$

Here E corresponds to the Young's modulus of the material, and C represents the compliance calculated as the reciprocal from the unloading slope of the samples during testing. All testing was conducted within the stated range of measurement validity of $0.3 \leq a/W \leq 0.8$. The strain gauges were calibrated and balanced at zero load and checked for measurement accuracy throughout the pre-cracking stage using optical microscopy techniques to verify and calibrate the system to ensure the calculated crack length accurately reflected the actual crack length.

Sinusoidal cyclic fatigue loading (tension-tension) was conducted using an electro-servo hydraulic MTS 810 testing machine (MTS Corporation, Eden Prairie, MN, USA) controlled by an Instron 8800 digital controller (Instron Corporation, Norwood, MA, USA). Prior to testing, all samples were fatigue pre-cracked in accordance with ASTM Standard E647 [24] at ambient temperature at a frequency 25 Hz (sine wave) under constant cyclic loading over a stress-intensity range ΔK = 11 to 2 MPa$\sqrt{m}$, where $\Delta K = K_{max} - K_{min}$, and the load ratio, the ratio of minimum load to maximum load, ranged from R = 0.1 to 0.7. Between pre-cracking steps, the crack path was visually checked for linearity and measured on both sides of the samples to ensure even and valid crack growth. Including notch, the final pre-crack lengths ranged from a_o ~3.9 to 4.2 mm (a/W ~ 0.31-0.34), as per standard requirements [24].

All fatigue-crack propagation testing was performed under load-shedding or constant load control conditions at a constant load ratio. Near-threshold testing was performed under load-shedding conditions in which the controller was automated to decrease the imposed load at a rate such that the normalized K-gradient remained above -0.08 mm^{-1}, as recommended in ASTM E647 [24]. The value of the ΔK_{th} fatigue threshold stress-intensity range was determined to be at the value of ΔK at which the growth rates were less than 10^{-11} m/cycle. Higher crack growth rates were characterized under constant load conditions, in which the amplitude of the alternating load was held constant, effectively increasing the stress-intensity range as the crack grew.

Fatigue-crack propagation testing, over the range 10^{-11} to 10^{-7} m/cycle, was performed at 25 Hz at temperatures of 293 K, 198 K and 77 K at load ratios of R = 0.1, 0.4 and 0.7. Tests at the two cryogenic temperatures were performed with immersion baths of liquid nitrogen and ethanol/dry-ice for 77 K and 198 K, respectively, with sufficient time allowed for sample and

strain gauge temperatures to equilibrate with the environment before the start of testing. The 293 K testing was performed in air under ambient laboratory conditions. All tests were performed continuously without interruption once started to maintain conditions and avoid any thermal cycling effects. Data are presented as log-log plots of the fatigue-crack growth rates da/dN as a function of ΔK, following a nominal Paris power-law formulation [25] where $da/dN \propto \Delta K^m$, where m is the Paris law exponent (typically measured in the mid-range of growth rates, *i.e.*, in this alloy above 10^{-9} m/cycle).

Near-threshold test specimens were further subjected to loading and unloading to estimate the extent of crack closure, K_{cl}, *i.e.*, the physical contact of the mating fracture surfaces, the crack experiences in the wake of the tip upon unloading of the sample. To measure closure for each sample, the sample was loaded uniaxially to a load corresponding to the maximum load at the threshold, and then unloaded to a load corresponding to the minimum loading with the resulting load-displacement curve recorded. These full loading-unloading cycles were repeated 5 times. The point at which the slope of the unloading curve changes was identified as the point at which the crack is closed as the fracture surfaces come into contact. As with most quantitative estimates of closure, this technique is approximate; however, the analysis was used to determine an approximate effective stress-intensity range actually experienced at the crack tip, where $\Delta K_{eff} = K_{max} - K_{cl}$, and where $K_{cl} > K_{min}$; where $K_{cl} < K_{min}$, $\Delta K_{eff} = \Delta K$. Full details of these procedures can be found elsewhere [26,27]. The loading cycles were performed, at each of the three test temperatures, in incremental steps corresponding to an increase in ΔK of 0.5 MPa$\sqrt{m}$ beginning at the threshold of the respective sample and the resultant load-displacement curves were plotted as described below.

2.2. Fractographic characterization

At the conclusion of the mechanical testing, fractographical analysis was performed to characterize the nature and mechanisms involved in crack propagation under the various conditions. Fracture surface characterization was performed on samples fatigued in tension to overload to expose the surface while maintaining surface features. Imaging was conducted in

secondary electron (SE) modes of a FEI Strata DB235 SEM (FEI Company, Hillsboro, OR, USA) and a JSM-7500F SEM (JEOL USA, Arvada, CO, USA) operated at 5-15 kV.

To specifically examine the crack path and the deformation mechanisms, in particular the occurrence of deformation twinning, in the frontal plastic zone and its wake, where the plastic-zone size, r_y, was estimated as $1/2\pi\ (K_{max}/\sigma_y)^2$ where σ_y is the yield strength, each fatigue tested DC(T) sample was longitudinally sliced into two metallurgical samples at the mid-plane section, and subsequently ground and polished sequentially using 1 μm polycrystalline diamond suspension and then a 0.05 μm alumina suspension. The final surface was analyzed using back-scattered electron (BSE) imaging and electron backscatter diffraction (EBSD) imaging was conducted after vibration polishing for 12 hr with the sample surface emerged in colloidal silica suspension. SE and BSE imaging were conducted by using a Hitachi S-4300SE/N scanning electron microscope, SEM (Hitachi America, Pleasanton, CA) operated at 10 kV. EBSD scans were performed along the crack path and in the vicinity of the crack tip on the polished mid-plane sections using the FEI Strata DB235 SEM operated at 20 kV using a TEAM™ EDAX analysis system (Ametek EDAX, Mahwah, NJ, USA). The SEM was equipped with an Orientation Imaging Microscopy (OIM) system (Ametek EDAX, Mahwah, NJ, USA), which enabled image post-processing using OIM Analysis v7 software. To specifically detect nano-twins, EBSD data were collected with the finest step size of 18 nm.

3. Results

While many metallic materials experience a degradation in damage-tolerance at low temperatures, the CrMnFeCoNi notably displays an increase in tensile strength and ductility [11,14,16,17]. Our previous fatigue-crack propagation studies on this alloy conducted at low load ratios (R = 0.1) noted a similar improvement of fatigue properties, specifically fatigue-crack propagation properties, as the temperature was lowered, which was particularly evident in the near-threshold regime [19]. In the present study, we extended the measurement of fatigue-crack propagation rates and ΔK_{th} threshold stress-intensity data down to 77 K and explicitly examined the role of load ratio. A plot of all collected fatigue-crack propagation data as a function of the

stress-intensity range for the Cantor alloy is shown in Figure 1; specific parameters measured from the data are listed in Table 1.

3.1. Fatigue-crack growth behavior

From Fig. 1 and Table 1, it can be seen that over the mid-range of growth rates above ~10^{-9} m/cycle, the Paris law exponents for all temperatures and load ratios were largely in the characteristic range of m ~ 2 to 4, although in general there was a marked trend of increasing fatigue-crack growth resistance, *i.e.*, lower growth rates, at a given ΔK, and higher values of the fatigue ΔK_{th} thresholds, at the lower temperatures. Indeed, threshold ΔK_{th} values, which ranged from 6.3 to 2.5 MPa$\sqrt{m}$ at load ratios between 0.1 and 0.7, were respectively 31% and 12% higher at 198 K than at 293 K (Fig. 2). As discussed elsewhere [19], such fatigue-crack growth rates in this high-entropy alloy are comparable to that of traditional metallic alloys with tensile strengths of the order of 1 GPa (for an extended discussion, see ref. [19]).

Additionally, we found a marked effect of increasing fatigue-crack growth rates with increasing load ratios, which became more prominent at near-threshold levels. Specifically, ΔK_{th} threshold values, in particular, were lower at increasing R; in fact, ΔK_{th} values were 2-3 times lower at $R = 0.7$ compared to $R = 0.1$ (Fig. 2). Such load-ratio dependent behavior is typical of most metallic alloys [25] and can generally be related to crack-tip shielding from fatigue crack closure effects [27-29], as discussed below.

It should also be noted that based on $da/dN \propto \Delta CTOD \propto \Delta K^2/\sigma_y E$, where CTOD is the crack-tip opening displacement, when σ_y is only weakly dependent on temperature, as in pure *fcc* metals, da/dN values for a given ΔK can be assumed to be similar at high R-ratios where crack closure can essentially be neglected. In our material, however, the differences in growth rates between room and liquid nitrogen temperatures, *e.g.*, at a ΔK of 5 MPa$\sqrt{m}$, the crack growth rate at R = 0.7 at 77K is approximately 1x10^{-9} m/cycle, whereas at 293K it is approximately 2x10^{-9} m/cycle (see Fig. 1), is likely associated with changes in σ_y, and to a lesser extent E, between these two temperatures.

3.2. Threshold and crack closure analysis

The most prevalent reason for the marked effect of load ratio on fatigue-crack growth rates, especially at near-threshold levels, is that of crack closure. As this phenomenon is dominated by shielding effects due to wedging between the crack flanks, *e.g.*, from corrosion debris (oxide-induced crack closure) and/or from crack surface asperities (roughness-induced crack closure), which act to reduce the effective stress-intensity *range* actually experienced at the crack tip, crack closure is exacerbated at low ΔK levels, where the crack-tip opening displacements (CTODs) are small and become comparable in dimension to the thickness of the "wedge", yet minimized at high positive load ratios where the minimum opening displacements are much larger, specifically where $K_{min} > K_{cl}$ [28]. On the simple assumption that the value of the closure stress intensity K_{cl}, and the effective stress intensity range at the threshold $\Delta K_{eff,th}$ are nominally constant and independent of R, we would expect the measured variation in ΔK_{th} thresholds to follow "Schmidt & Paris type" behavior [29]. Specifically, below a critical load ratio where $K_{cl} = K_{min}$ (this is typically of the order of $R \sim 0.4$-0.5), the ΔK_{th} threshold should decrease with increasing R whereas the threshold K_{max} should remain roughly constant (this is the regime where closure is active as $K_{cl} > K_{min}$); above this critical R value though (where closure is inactive as $K_{cl} < K_{min}$), the value of ΔK_{th} threshold should reach a lower-bound "plateau" whereas the $K_{max,th}$ threshold should increase as R tends to unity. This type of variation in fatigue threshold values and how it relates to the presence of crack closure phenomena is described in further detail in ref. [30]. Although we have only tested three different load ratios at each temperature, our threshold measurements for this high-entropy alloy are not inconsistent with this hypothesis, as shown in Fig. 2.

Comparison of these ΔK_{th} fatigue thresholds with those in steels and other engineering metallic alloys at comparable strength levels [26-31] suggests that the values measured in this study, and previously [19], for the CrMnFeCoNi HEA are comparable in magnitude.

To provide some quantitative evidence for these explanations for the variation in fatigue thresholds in the Cantor alloy based on crack closure, K_{cl} closure stress intensities that were measured at near-threshold levels on samples tested at 293 K and 198 K, are summarized in Table 1. It is evident that crack closure levels are far higher at low load ratios, as expected. Moreover, the effective $\Delta K_{eff,th}$ thresholds appear to be roughly constant, again consistent with our

observations of the marked effect of load ratio on the near-threshold fatigue behavior being associated with a crack closure effect. With regards to the trends in fatigue properties with temperature, the data show that crack closure is observed at R = 01 and 0.4 but not at R = 0.7 in samples tested at 198 K. In both temperature ranges, crack closure appears to play a major role in the near-threshold fatigue behavior of this alloy.

However, pertinent questions that remain are whether this closure effect can be associated with fracture surface roughness, which is the most ubiquitous form of fatigue crack closure in metallic materials, whether such phenomena can explain the observed increase in ΔK_{th} thresholds in this HEA at cryogenic temperatures, and whether deformation twinning, which is so prevalent during overload fracture in this alloy at 77 K [16,17], may play an active role during fatigue-crack growth. To investigate these issues, we investigate crack trajectories and corresponding fracture surface morphologies, as described below.

3.3. Fractography

Fractography was performed using scanning electron microscopy on the fracture surfaces of representative samples. Images depicting regions at approximately ΔK ~ 12 MPa√m are shown in Fig. 3 and are oriented with the general crack propagation direction from the top to the bottom of the micrographs. For tests at low load ratios, a transition from transgranular to intergranular fracture behavior, from relatively smooth fracture surfaces to coarser, facet-like features, was seen for the lower crack-growth rates as the temperature was reduced from 293 K to 198 K [19]. This intergranular behavior is particularly visible in Figs. 3b and 3e, in which the feature sizes of the facet-like structures correspond to some small fraction of the grain size, suggesting a fracture path along the grain boundaries at 198 K; in contrast, the corresponding 293 K fracture surfaces, imaged Figs. 3c and 3f, show much smaller, more irregular surface features that may correspond to slip or other plastic fracture behavior. Such behavior, which purports that the fatigue fracture surfaces become rougher at the lower temperature, is consistent with the higher measured closure values and our observations of higher ΔK_{th} thresholds at 198 K as compared to 293 K as demonstrated in Fig. 1. This general trend is observed to continue as the temperature is lowered further to 77 K as shown in Fig. 3, though the facets are somewhat more obscured. Together, these

images depict a greater degree of plastic deformation within samples subject to comparable stress intensities at higher temperatures and, especially at lower ΔK levels, to a rougher, more faceted, intergranular fracture mode at cryogenic temperatures. Additionally, with increasing ΔK levels, especially as the R-ratio is increased, evidence of local cyclic plasticity, *e.g.*, in the form of markedly visible fatigue striations (Fig. 4), becomes more prominent.

As with many metallic alloys [26-28], one may conclude that the influence of both temperature and load ratio on fatigue-crack propagation behavior in this alloy likely result primarily from closure effects, principally motivated by such fracture surface roughness. By promoting premature contact of the crack surfaces due to their rough morphology during the unloading cycle, roughness-induced crack closure acts to increase the effective minimum stress intensity, thereby reducing the effective stress-intensity range actually experienced at the crack tip. Such roughness has a larger effect at near-threshold levels, where the cyclic crack-tip opening displacements ΔCTODs ($\sim\Delta K^2/2\sigma_y E$) are smaller, which on the basis of our K_{cl} measurements (Table 1) appears to account for the higher ΔK_{th} thresholds at lower temperatures. Furthermore, the closure concept is consistent with the lesser effect of temperature on ΔK_{th} thresholds at high load ratios, where the maximum CTODs are far larger, as shown in Table 1. This represents the generally accepted reason for the decrease in ΔK_{th} thresholds with increasing R [28-30].

3.4. Crack path studies

To further investigate the potential deformation mechanisms at play during fatigue-crack growth in the Cantor alloy, EBSD imaging was performed along the central (mid-thickness) cross-section of fatigued samples, with a particular focus on the crack path and the presence, or absence, of deformation nano-twins in the strained regions in the vicinity of the crack tip. Nano-twinning has been identified as a prime mechanism associated with the exceptional toughness of this alloy at cryogenic properties with a greater propensity to occur at higher strains and lower temperatures where strength levels are higher [16,17]; there is little evidence of such twinning during deformation in CrMnFeCoNi at ambient temperatures, except at high strains just prior to fracture. As no evidence of twinning during fatigue-crack growth was seen at ΔK levels less than 10 MPa$\sqrt{m}$ for temperatures at or above 198 K in our previous study [19], we sought here to extend

these observations down to 77 K and to higher stress-intensity ranges at higher load ratios (to maximize the local crack-tip stresses).

BSE and EBSD images in Fig. 5 show the microstructure features taken in the crack-tip region at 77 K under $R = 0.1$ and $R = 0.7$ with ΔK levels of 29 MPa√m and 20 MPa√m, respectively (corresponding K_{max} values at $R = 0.1$ and 0.7 were 32 and 67 MPa√m). Here, the entire imaged region may be presumed to have experienced deformation, due to the large size of the maximum plastic zone r_y, which was approximately ~287 μm and ~1.23 mm, respectively at these two $R = 0.1$ and 0.7 loading conditions.

As revealed in BSE and EBSD images, fatigue-crack propagation at both R-ratios is largely transgranular at higher ΔK levels with an increasing incidence of rougher, more facetted, intergranular-type fracture at lower, near-threshold levels. BSE scans reveal the formation of dislocation cells and deformation nano-twins in the wake of the propagated crack within a region of 1~3 grains. Most importantly, EBSD inverse pole figure (IPF) maps overlaid with image quality (IQ) maps[1] confirm the presence of the deformation-induced nano-twinning during fatigue cracking at 77 K [1].[2] This conclusion is further verified by the line scans across the twin boundaries, showing a typical 60° misorientation between the twin domain and the parent grain domain. Compared to crack growth at $R = 0.1$, the nano-twins and dislocation cells associated with crack growth at $R = 0.7$ are more pronounced, with the thickness of the measurable nano-twins roughly 50% wider at $R = 0.7$ than at $R = 0.1$; this is likely due to the far higher K_{max} value of ~67 MPa√m. We conclude that deformation-induced nano-twinning is active in the process of cyclic deformation during fatigue-crack propagation in the Cantor alloy at liquid-nitrogen temperatures, although there is little evidence for this under ambient-temperature conditions.

4. Discussion

[1] Image quality IQ maps measure the sharpness of the Kikuchi bands collected at each EBSD scan point [32]. They are useful in visualizing the microstructural features that cause poor band contrast, such as small pores/inclusions and phase/grain/twin boundaries.

[2] Note that there is always evidence of a few annealing twins. However, these can be readily distinguished from deformation-induced nano-twins as the annealing twins are far larger with widths of several micrometers.

The CrMnFeCoNi alloy, developed by Cantor and coworkers [2], is almost certainly the most studied high-entropy alloy to date, principally because it has been shown to display exceptional mechanical properties of high strength, ductility and fracture toughness, which are all increased at cryogenic temperatures [3,14-17]. Although the mechanisms underlying such behavior are complex involving a synergy of differing deformation processes [16,33], a prime mechanism appears to involve the onset of deformation nano-twinning at lower temperatures which serves to enhance strain hardening to promote strength and ductility, the latter by delaying the onset of plastic instability or necking [14-17]. In light of this, it is of interest that we show here that similarly the fatigue-crack propagation resistance, specifically the value of the ΔK_{th} fatigue threshold, is also increased at cryogenic temperatures in this alloy. However, this effect, we believe, derives from a completely different mechanism, that of the enhancement of (roughness-induced) crack closure at lower temperatures due to the onset of a rougher, more facetted, intergranular fatigue fracture mode. Irrespective of the prevailing mechanisms though, the damage-tolerant properties of the CrMnFeCoNi high-entropy alloy, with respect to both subcritical cracking (fatigue) resistance and the crack-initiation and growth fracture toughnesses at tensile strengths exceeding 1 GPa [14-19], are exceptional and comparable, or even exceed, the best metallic structural materials reported to date. Indeed, the Cantor alloy shows outstanding promise for numerous structural applications, particularly under cryogenic conditions.

5. Conclusions

Based on an experimental study of fatigue-crack propagation in the equiatomic Cantor high-entropy alloy, comprising a face-centered cubic CrMnFeCoNi solid solution with ~7 μm grain size, as a function of load ratio (R = 0.1 to 0.7) at temperatures between 293 and 77 K, the following conclusions can be made:

- In the mid-range of growth rates, above 10^{-9} m/cycle, the Paris power-law exponents for all temperatures and load ratios were largely in the characteristic range of m ~ 2 to 4, consistent with observations of fatigue striations. As noted previously, such fatigue-crack growth behavior in this HEA is comparable to that of traditional metallic alloys with tensile strengths of the order of 1 GPa.

- Fatigue-crack propagation resistance, in terms of lower growth rates at a given ΔK, and higher values of the ΔK_{th} fatigue thresholds, was increased with decrease in temperature, with the effect being progressively enhanced at near-threshold levels. Indeed, ΔK_{th} values, which ranged from 6.3 to 2.5 MPa$\sqrt{m}$ at load ratios between 0.1 and 0.7, were respectively 31% and 12% higher at 198 K than at 293 K. Again, these values are typical for traditional metallic alloys at this strength range.
- Crack closure was found to occur during fatigue-crack growth, and was assessed using compliance techniques in measurements of the closure stress intensity, K_{cl}. As measured closure levels were higher at the lower temperatures, in accordance with crack wedging due to a more facetted intergranular crack path, we believe that the more prominent occurrence of this mode of crack-tip shielding was the main factor underlying the increased fatigue resistance of this alloy at the lower temperatures. This conclusion is consistent with observations that the beneficial effect of cryogenic temperatures was enhanced at lower growth rates where the crack-tip opening displacements are smaller.
- Characteristic of most metallic materials, crack-growth rates were increased with increase in load ratio, with the effect being more pronounced at progressively decreasing growth rates. Indeed, for temperatures of 293 and 198K, values of the ΔK_{th} fatigue thresholds were some 2 to 3 times higher at R = 0.1 than at R = 0.7. Again, such behavior was found to be consistent with crack closure phenomena, principally due (at a given ΔK) to the larger crack-tip opening displacements generated at high load ratios.
- Although not observed at ambient temperatures, evidence was found for cyclic deformation-induced nano-twinning during fatigue-crack propagation in the CrMnFeCoNi alloy at temperatures as low as 77 K and load ratios of 0.1 and 0.7. Compared to R = 0.1, nano-twins were more pronounced and thicker at R = 0.7, likely due to the much higher K_{max} values under high R loading.

Acknowledgements

This study was conducted by the Mechanical Properties of Materials program (KC13) at the Lawrence Berkeley National Laboratory (LBNL), supported by the U.S. Department of Energy, Office of Science, Office of Basic Energy Sciences, Division of Materials Sciences and Engineering under contract no. DE-AC02-05-CH11231. E.P.G. was also supported by the Materials Sciences and Engineering Division of the Department of Energy, Office of Science, Office of Basic Energy Sciences through the Materials Science and Technology Division at the Oak Ridge National Laboratory. K.V.S.T. acknowledges salary support from a Natural Science Foundation Graduate Fellowship, under NSF GRFP grant no. 1106400, and G.L. acknowledges funding from the German Research Foundation (DFG) through project LA 3607/1-1. Electron microscopy was carried out at LBNL's Molecular Foundry supported by the Office of Science, Office of Basic Energy Sciences, of the U.S. Department of Energy under contract no. DE-AC02-05-CH11231.

References

[1] W. Li, P. K. Liaw, Y. Gao, Fracture resistance of high entropy alloys: a review, Intermetallics 99 (2018) 69-83, http://dx.doi.org/10.1016/j.intermet.2018.05.013.

[2] B. Cantor, I. T. H. Chang, P. Knight, A. J. B. Vincent, Microstructural development in equiatomic multicomponent alloys, Mater. Sci. Eng. A 375-377 (2004) 213-218, http://dx.doi.org/doi:10.1016/j.msea.2003.10.257.

[3] A. Gali, E. P. George, Tensile properties of high- and medium-entropy alloys, Intermetallics, 39 (2013) 74-78, http://dx.doi.org/10.1016/j.intermet.2013.03.018.

[4] J. W. Yeh, S. K. Chen, S. J. Lin, J. Y. Gan, T. S. Chin, T. T. Shun, C. H. Tsau, S. Y. Chang, Nanostructured high-entropy alloys with multiple principle elements: Novel alloy design concepts and outcomes, Adv. Eng. Mater. 6 (2004) 299-303, http://dx.doi.org/10.1002/adem.200300567.

[5] J. Chen, J. Chen, X. Zhou, W. Wang, B. Liu, Y. Lv, W. Yang, D. Xu, Y. Lu, A review on fundamental of high entropy alloys with promising high-temperature properties, J. Alloys Compd. 760 (2018) 15-30, http://dx.doi.org/10.1016/j.jallcom.2018.05.067.

[6] Y. F. Ye, Q. Wang, J. Lu, C. T. Liu, Y. Yang., High-entropy alloy: Challenges and prospects, Mater. Today 19 (6) (2016) 349-362, http://dx.doi.org/10.1016/j.mattod.2015.11.026.

[7] Y. Zhang, T. T. Zuo, Z. Tang, M. C. Gao, K. A. Dahman, P. K. Liaw, Z. P. Lu, Microstructures and properties of high-entropy alloys, Prog. Mater. Sci. 61 (2014) 1-93, http://dx.doi.org/10.1016/j.pmatsci.2013.10.001.

[8] E. J. Pickering, N. G. Jones, High-entropy alloys: A critical assessment of their founding principles and future prospects, Int. Mater. Rev. 61 (2016) 1743-2804, http://dx.doi.org/10.1080/09506608.2016.1180020.

[9] Z. Li, Z. S. Zhao, R. O. Ritchie, M. A. Meyers. Mechanical properties of high-entropy alloys with emphasis on face-centered cubic alloys. Progr. Mater. Sci. 102 (2019): 296–345. https://doi.org/10.1016/j.pmatsci.2018.12.003.

[10] J. W. Yeh, Physical metallurgy of high-entropy alloys, JOM 67 (2015) 2254-2261, http://dx.doi.org/10.1007/s11837-015-1583-5.

[11] F. Otto, Y. Yang, H. Bei, E. P. George, Relative effects of enthalpy and entropy on the phase stability of equatomic high-entropy alloys, Acta Mater. 61 (2013) 2628-2638, http://dx.doi.org/10.1016/j.actamat.2013.01.042.

[12] C. C. Tasan, Y. Deng, K. G. Pradeep, M. J. Yao, H. Springer, D. Raabe, Composition dependence of phase stability, deformation mechanisms, and mechanical properties of the CoCrFeMnNi high-entropy alloy system, JOM 66 (2014) 1993-2001, http://dx.doi.org/10.1007/s11837-014-1133-6.

[13] C. G. Schön, T. Duong, Y. Wang, R. Arróyave, Probing the entropy hypothesis in highly concentrated alloys, Acta Mater. 148 (2018) 263-279, http://dx.doi.org/10.1016/j.actamat.2018.01.028.

[14] B. Gludovatz, E. P. George, R. O. Ritchie, Processing, microstructure and mechanical properties of the CrMnFeCoNi high-entropy alloy, JOM 67 (2016) 2262-2270, http://dx.doi.org/10.1007/s11837-015-1589-z.

[15] S. J. Sun, Y. Z. Tien, H. R. Lin, H. J. Yang, X. G. Dong, Y. H. Wang, Z. F. Zhang, Achieving high ductility in the 1.7 GPa grade CoCrFeMnNi high-entropy alloy at 77 K, Mater. Sci. Eng. A 740-741 (2019) 336-341, http://dx.doi.org/10.1016/j.msea.2018.10.094.

[16] B. Gludovatz, A. Hohenwarter, D. Cartoor, E. H. Chang, E. P. George, R. O. Ritchie, A fracture-resistant high-entropy alloy for cryogenic applications, Science 345 (2014) 1153-1158, http://dx.doi.org/10.1126/science.1254581.

[17] F. Otto, A. Dlouhy, Ch. Somsen, H. Bei, G. Eggeler, E. P. George, The influences of temperature and microstructure on the tensile properties of CoCrFeMnNi high-entropy alloy, Acta Mater. 61 (2013) 5743-5755, http://dx.doi.org/10.1016/j.actamat.2013.06.018.

[18] N. Stepanov, M. Tikhonovsky, N. Yurchenko, D. Zyabkin, M. Klimova, S. Zherebtsov, A. Efimov, G. Salishchev, Effect of cryo-deformation on structure and properties of CoCrFeNiMn high-entropy alloy, Intermetallics 55 (2015) 8-17, http://dx.doi.org/10.1016/j.intermet.2014.12.004.

[19] K. V. S. Thurston, B. Gludovatz, A. Hohenwarter, G. Laplanche, E. P. George, R. O. Ritchie, Effect of temperature on the fatigue-crack growth behavior of the high-entropy alloy CrMnFeCoNi, Intermetallics 88 (2017) 65-72, http://dx.doi.org/10.1016/j.intermet.2017.05.009.

[20] M. Seifi, D. Li, Z. Yong, P. K. Liaw, J. J. Lewandowski, Fracture toughness and fatigue crack growth behavior of as-cast high-entropy alloy, JOM 67 (2015) 2288-2295, http://dx.doi.org/10.1007/s11837-015-1563-9.

[21] M. A. Hemphill, T. Yuan, G. Y. Wang, J. W. Yeh, C. W. Tsai, A. Chuang, P. K. Liaw, Fatigue behavior of $Al_{0.5}$CoCrCuFeNi high entropy alloys, Acta Mater. 60(16) (2012) 5723-5734, http://dx.doi.org/10.1016/j.actamat.2012.06.046.

[22] G. Laplanche, O. Horst, F. Otto, G. Eggeler, E. P. George, Microstructural evolution of a CoCrFeMnNi high-entropy alloy after swaging and annealing, J. Alloys Compd. 647 (2015) 548-57, http://dx.doi.org/10.1016/j.jallcom.2015.05.129.

[23] C. J. Gilbert, J. M. McNaney, R. H. Dauskardt, R. O. Ritchie, Back-face strain compliance and electrical-potential crack length calibrations for the disk-shaped compact-tension DC(T) specimen, J. Test. Eval. 22 (1994) 117-120, http://dx.doi.org/10.1520/jte12644j.

[24] ASTM Standard E647, Standard test method for measurement of fatigue crack growth rates, ASTM International, West Conshohocken, PA (2013), www.astm.org.

[25] P. C. Paris, F. Erdogan, A critical analysis of crack propagation laws, ASME, J. Basic Eng. 85(4) (1963) 528-533, http://dx.doi.org/10.1115/1.3656900.

[26] R. O. Ritchie, W. Yu, Short crack effects in fatigue: A consequence of crack tip shielding, in Small Fatigue Cracks, R. O. Ritchie and J. Lankford, eds., TMS-AIME (1986) 167-189.

[27] K. T. Venkateswara Rao, W. Yu, R. O. Ritchie, Fatigue crack propagation in aluminum-lithium alloy 2090: Part 1: Long crack behavior, Metall. Mater. Trans. A 19A(3) (1988) 549-561, http://dx.doi.org/10.1007/BF02649269.

[28] R. O. Ritchie, Mechanisms of fatigue crack propagation in metals, ceramics and composites: Role of crack-tip shielding, Mater. Sci. Eng. A 103 (1988) 15-28, http://dx.doi.org/10.1016/0025-5416(88)90547-2.

[29] R. A. Schmidt, P. C. Paris, Threshold for fatigue crack propagation and effects of load ratio and frequency, in Progress in Crack Growth and Fracture Toughness Testing, ASTM STP 536 (1973) 79-94, American Society for Testing and Materials, Philadelphia, PA.

[30] B. L. Boyce, R. O. Ritchie, Effect of load ratio and maximum stress intensity on the fatigue threshold in Ti-6Al-4V, Eng. Fract. Mech. 68 (2001) 129-147, http://dx.doi.org/10.1016/S0013-7944(00)00099-0.

[31] R. O. Ritchie, Near-threshold fatigue crack propagation in steels, Intl. Metals Rev. 24 (1979) 205-230, http://dx.doi.org/10.1179/imtr.1979.24.1.205.

[32] R. A. Schwarzer, J. Sukkau, Electron back scattered diffraction: Current state, prospects and comparison with x-ray diffraction texture measurement, Banaras Metall., 18 (2013) 1-11.

[33] Z-J. Zhang, M. M. Mao, J. Wang, H. Tian, B. Gludovatz, Z. Zhang, S. X. Mao, E. P. George, Q. Yu, R. O. Ritchie, Nanoscale origins of the damage tolerance of the high-entropy alloy CrMnFeCoNi, Nature Comm. 6 (2015) 10143, https://doi.org/10.1038/ncomms10143.

Table 1. Summary of fatigue-crack growth, threshold values and crack closure measurements for the CrMnFeCoNi HEA, extracted from Figs. 1, 2.

Temp.	Load Ratio (R)	Paris Law exponent (m)	Threshold (ΔK_{th}) [MPa√m]	$CTOD_{max}$ [nm]	Crack Closure (K_{cl}) [MPa√m]	$\Delta K_{th,eff}$ [MPa√m]	Plastic-zone size (r_y) [μm]
293 K	0.1	3.5	4.8	160	1.38	3.95	27
	0.4	2.8	2.6	105	-	2.6	18
	0.7	2.6	2.5	390	-	2.5	66
198 K	0.1	4.5	6.3	210	2.15	4.85	29
	0.4	3.4	4.8	275	2.7 - 3.4	4.6 - 5.3	38
	0.7	3.1	3.5	585	-	3.5	81
77 K	0.1	2.9					
	0.4	2.3					
	0.7	2.3					

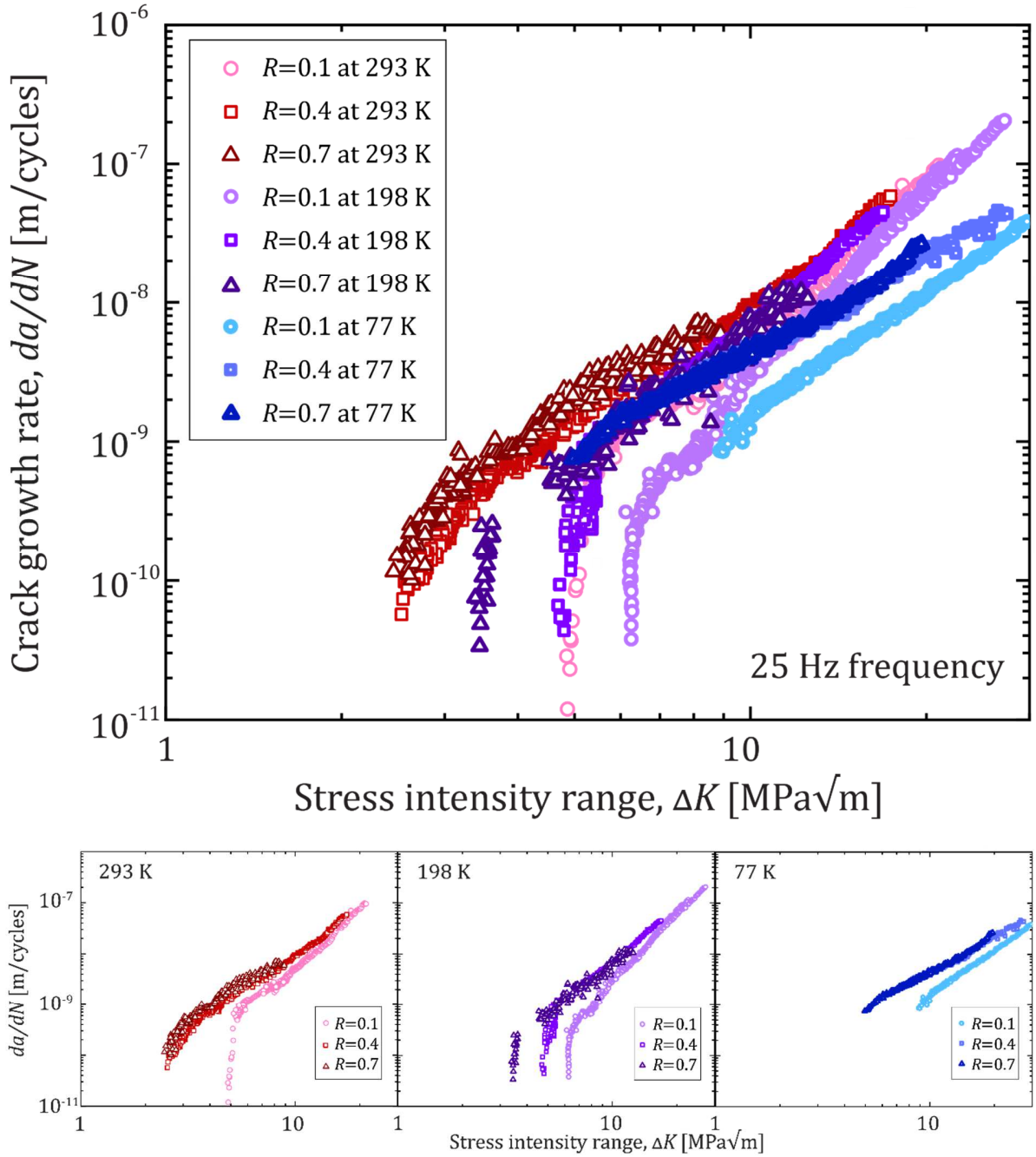

Figure 1. Fatigue-crack growth rates as a function of the stress-intensity range for the CrMnFeCoNi HEA under various testing conditions. Testing was conducted over three temperature ranges between ambient (293 K) and liquid-nitrogen temperature (77 K) at load ratios of R = 0.1, 0.4, and 0.7 at 25 Hz. Tests at 77 K were limited to growth rates above the ~10^{-9} m/cycle regime, while testing at 293 K and 198 K was performed until the fatigue threshold stress intensity was reached. A direct comparison of the crack-propagation curves characterizing these various testing parameters indicates an increase in the value of the ΔK_{th} fatigue threshold as both temperature and load ratio were decreased.

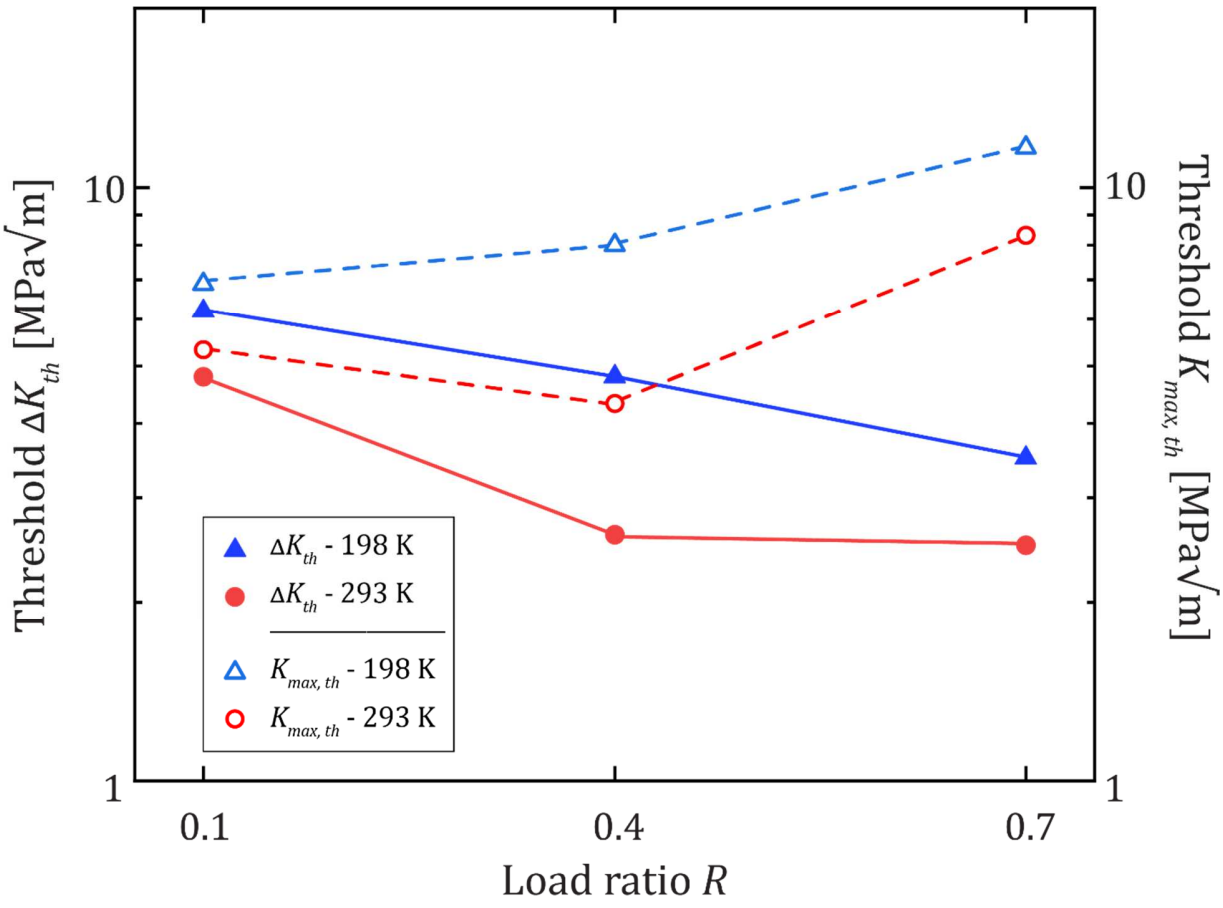

Figure 2. Variation in fatigue threshold values, in terms of both ΔK_{th} and $K_{max,th}$ thresholds, in the CrMnFeCoNi HEA as a function of load ratio R between 293 K and 198 K. ΔK_{th} thresholds tend to decrease with decreasing R, whereas the $K_{max,th}$ thresholds generally are increased, consistent with Schmidt & Paris-type behavior based on crack closure concepts [29,30].

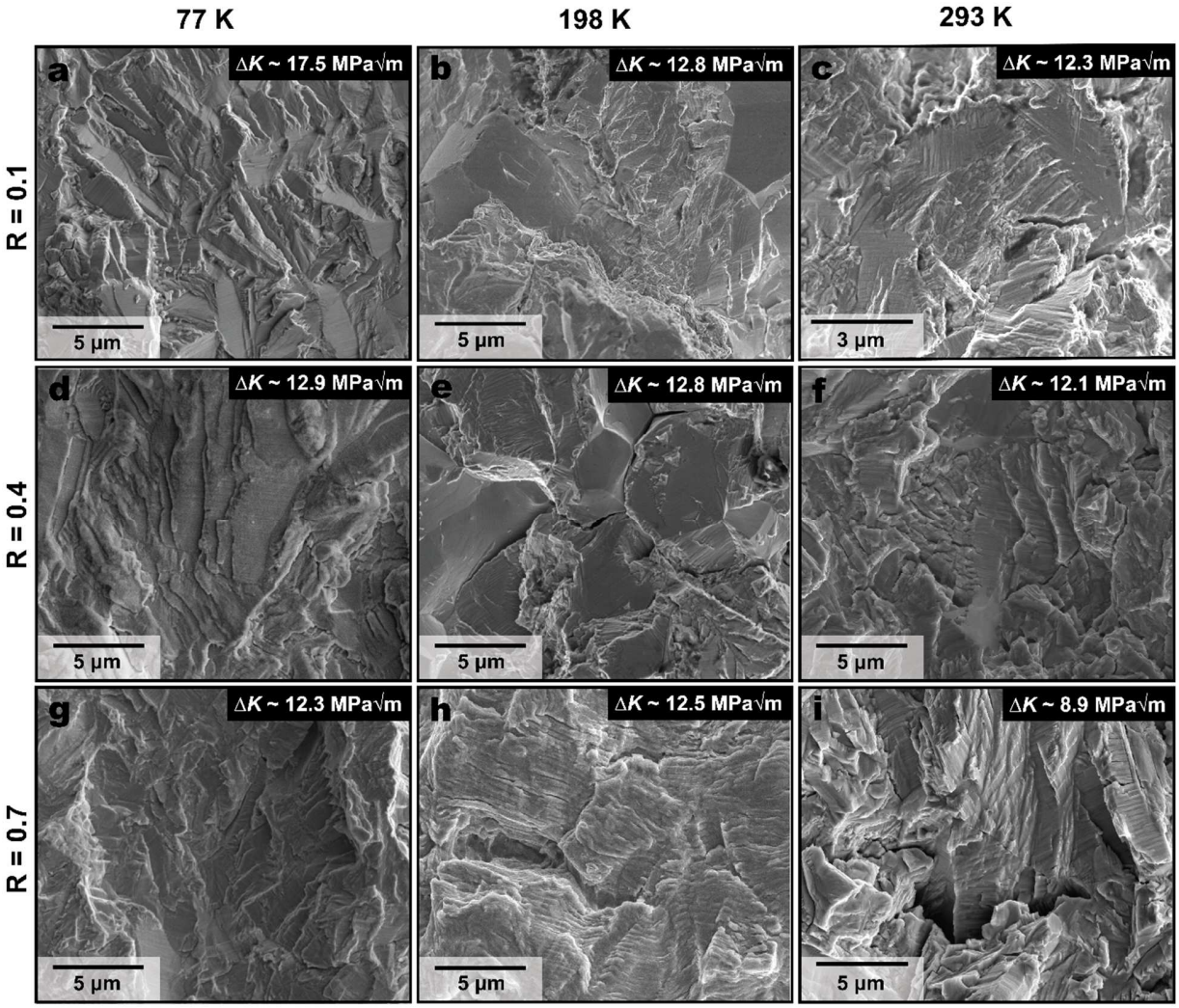

Figure 3. Overview of fractography for all nine testing conditions at a moderately high Δ*K* ~ 8 to 17 MPa√m for fatigue-crack growth in the CrMnFeCoNi HEA. A greater degree of facet-like features is seen at lower temperatures, particularly lower growth rates, with an increasing degree of transgranular fracture at higher Δ*K* levels. In general, increases in *R* and in temperature both correlate with a greater degree of plastic deformation of the fracture surfaces as characterized by an increasing prominence of fatigue striations.

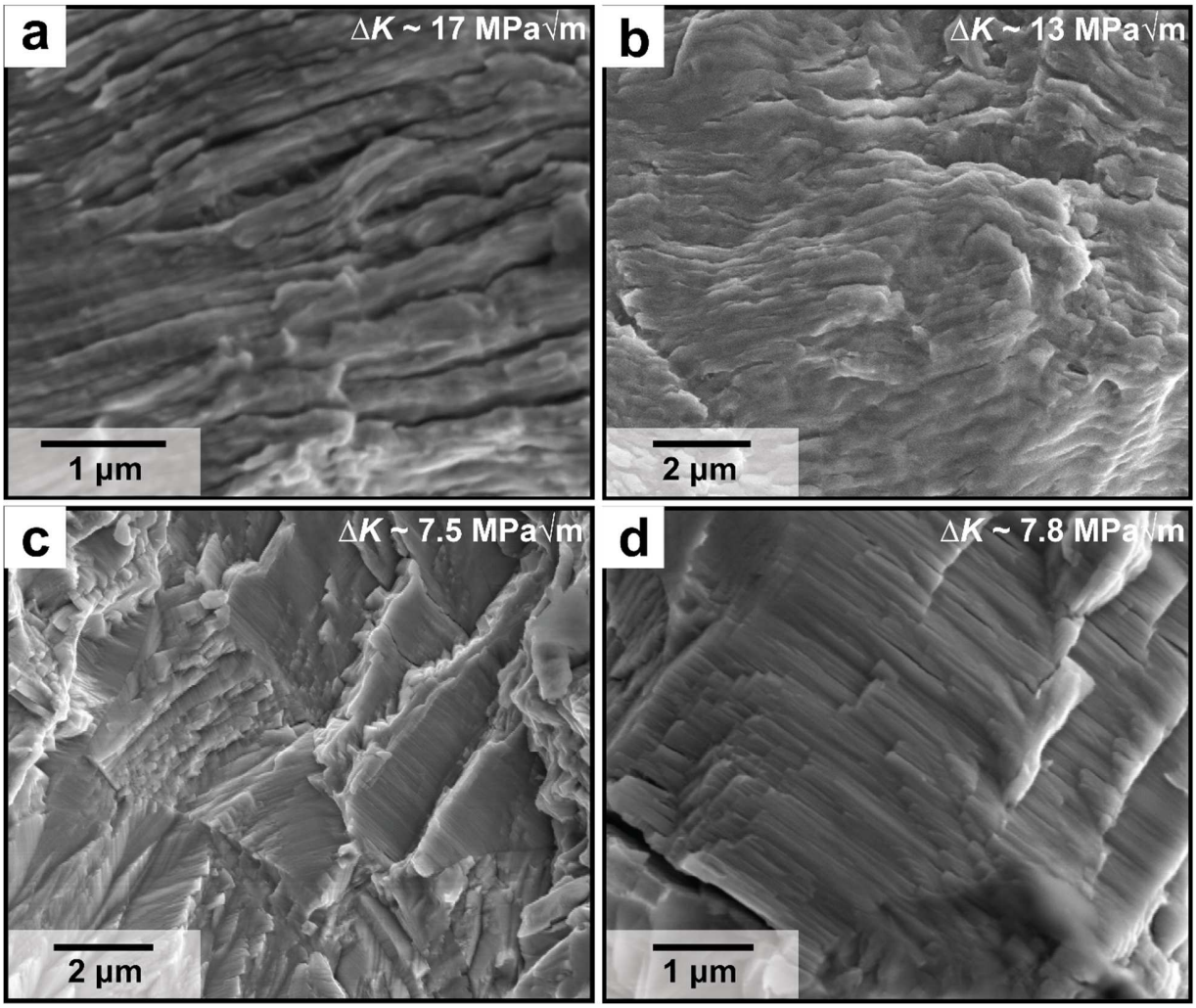

Figure 4. Striations and other microfeatures observed in higher *R*-ratio fatigue-crack growth testing of the CrMnFeCoNi HEA. Images (a) and (b) are 198 K tested samples at $R = 0.4$ and 0.7, respectively; images (c) and (d) are 293 K at $R = 0.4$ and 0.7, respectively. Striations featured prominently on the fracture surfaces of samples of all loading states, with particular prominence at higher ΔK levels, as this corresponds to higher crack-growth rates and thus larger striation spacings. Additionally, striations were found at lower ΔK levels at ambient temperature, and again appeared to be more prominent at the higher *R*-ratios.

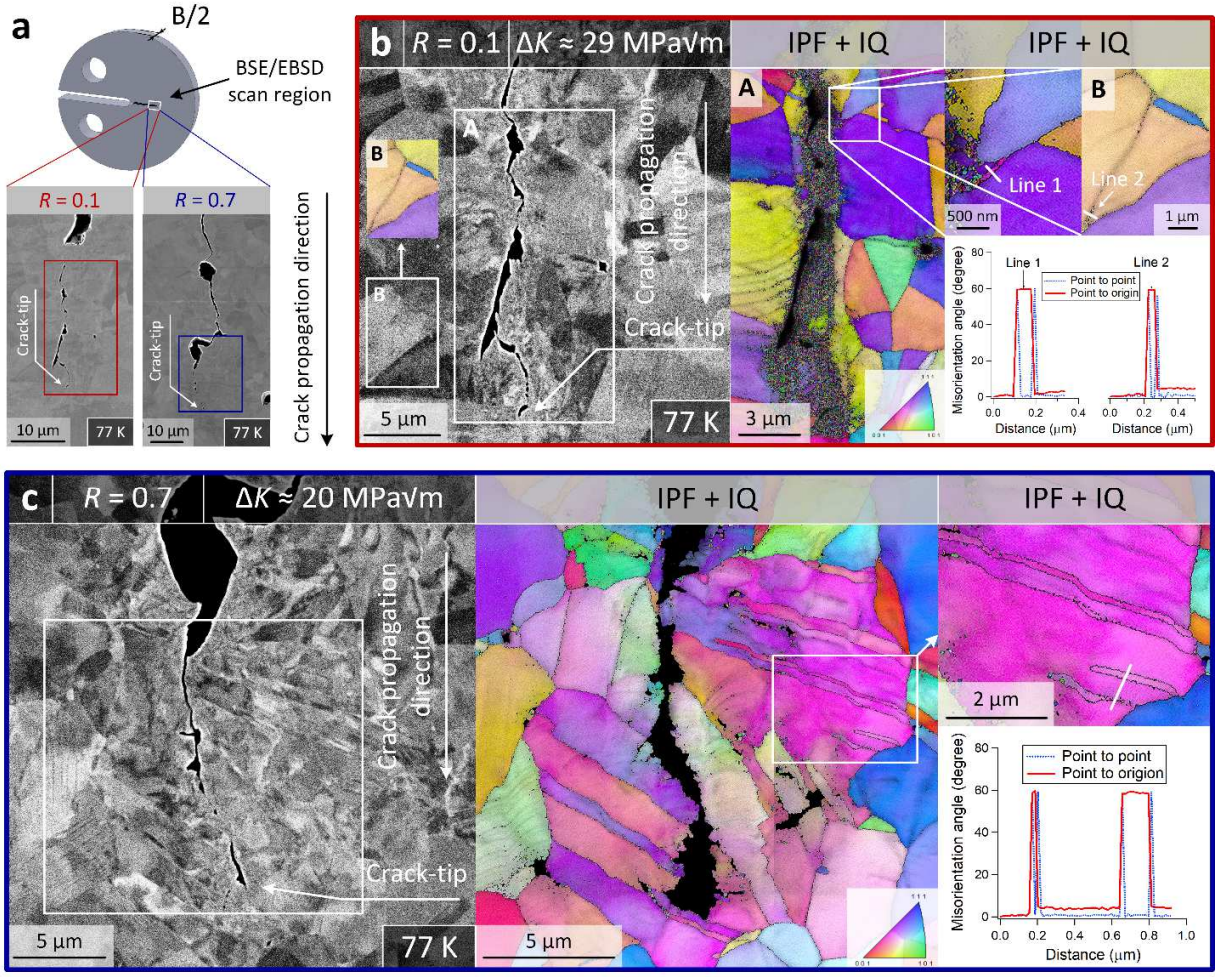

Figure 5. Deformation mechanisms in the vicinity of the crack tip in the CrMnFeCoNi high-entropy alloy (HEA) fatigue tested under *R*-ratios of 0.1 and 0.7 at 77 K. (a) Low-magnification secondary electron (SE) images captured in the crack-tip regions on the sliced mid-plane section of the C(T) specimen. (b) High-magnification back-scattered electron (BSE) images and electron-backscatter diffraction (EBSD) scans taken from the sample subjected to $R = 0.1$ with $\Delta K \approx 29$ MPa√m ($K_{max} \approx 32$ MPa√m). At higher ΔK levels, fracture is predominately trangranular, but an intergranular faceted mode of fracture becomes more prominent as the growth rates are reduced. BSE scans reveal the formation of dislocation cells and deformation nano-twins in the wake of the propagated crack within a region of 1~3 grains. The EBSD image, which is an overlaid map of inverse pole figure (IPF) and image quality (IQ) clearly shows deformation-induced nano-twinning at 77 K. Nano-twinning is confirmed by line scans across the twin boundaries, showing the 60° misorientation angle between the twin domain and the parent grain domain. (c) Corresponding BSE and EBSD images taken from the sample subjected to $R = 0.7$ with $\Delta K \approx 20$ MPa√m show pronounced nano-twinning and dislocation cells formed in the wake of the propagated crack.